NANO LETTERS

Letter

pubs.acs.org/NanoLett

Unravelling Nonlinear Spectral Evolution Using Nanoscale Photonic Near-Field Point-to-Point Measurements

Matthias Wulf,* Daryl M. Beggs, Nir Rotenberg, and L. Kuipers

Center for Nanophotonics, FOM Institute for Atomic and Molecular Physics (AMOLF), Science Park 104, 1098XG, Amsterdam, The Netherlands

Supporting Information

ABSTRACT: We demonstrate nanoscale photonic point-to-point measurements characterizing a single component inside an all-optical signal-processing chip. We perform spectrally resolved near-field scanning optical microscopy on ultrashort pulses propagating inside a slow light photonic crystal waveguide, which is part of a composite sample. A power study reveals a reshaping of the pulse's spectral density, which we model using the nonlinear Schrödinger equation. With the model, we are able to identify the various physical processes governing the nonlinear pulse propagation. Finally, we contrast the near-field measurements with transmission measurements of the complete composite sample to elucidate the importance of gaining local information about the evolution of the spectral density.

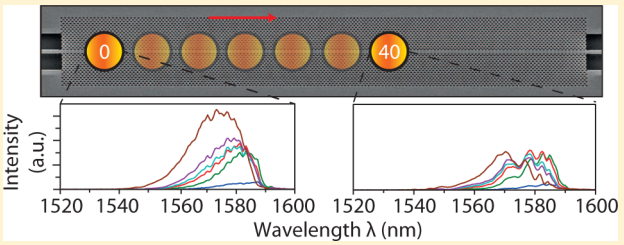

KEYWORDS: *Near-field spectroscopy, integrated nanophotonics, nonlinear optics, slow light, photonic crystal*

The ever increasing demands for speed in telecommunication has led researchers to develop a broad variety of all-optical signal-processing elements such as switches,[1] demultiplexers,[2] buffer lines,[3,4] dispersion compensators,[5] or signal regenerators.[6,7] Many of these devices were demonstrated with photonic crystal (PhC) waveguides,[8] which have emerged as a promising platform for integrated photonic circuits[9] due to their high mode confinement[8] and the freedom to design the dispersion of the guided mode.[10,11] Furthermore, these structures can support a guided mode featuring a high group index that has been shown to enhance light-matter interaction[12−15]and hence enabling more compact device designs.

Nonlinear optical effects, which allow for the control of light with light,[16] are crucial for all-optical signal-processing. Conventionally, nonlinear optical properties of a device (e.g., a waveguide) are experimentally determined by analyzing the properties of a transmitted laser pulse for different input powers.[17−20] In contrast to the linear optics regime, where only the characteristics of the different devices inside the circuit matter, in the nonlinear regime the order in which the different components are arranged is also crucial. Thus, it is a challenging task to extract the characteristics of individual components of an integrated photonic circuit from a single transmission measurement. What is missing is a photonic analogue to electronic point-to-point measurements,[21] which would characterize the performance of each component within a nanophotonic chip, instead of measuring all effects accumulated in the sample at the same time.

Near-field microscopy, which allows for local optical measurements with a resolution beyond the diffraction limit[22] has the potential to address this need. The characterization of integrated photonic devices by near-field scanning optical microscopy (NSOM) involved mapping the nanoscopic electric field profile of modes in waveguiding structures.[23,24] Furthermore, NSOM measurements have visualized low intensity pulses propagating inside photonic structures, both in the time domain[25,26] and spectrally[27] in the linear optical regime. Alternatively, near-field microscopy was used to gain local temporal or spectral information of processes such as photoluminescence from J-aggregates,[28] quantum wires,[29] or quantum wells.[30] However, local spectral point-to-point measurements on a single component on a photonic chip that, for example, characterize a high intensity ultrashort pulse propagating in the nonlinear regime, are missing so far.

In this Letter, we demonstrate how a NSOM technique can be used to track the spectral evolution of such a pulse inside a single component of a more complex photonic chip. We measure the changes of the spectral density as the ultrashort pulse propagates through a slow light PhC waveguide by monitoring the shape, peak amplitude, mean wavelength, and width of the laser spectrum. Numerical calculations reveal that the spectral reshaping is caused by the interplay between dispersion, nonlinear, and free-carrier effects. Finally, we show that the information gained by NSOM allows us to model the pulse propagation inside the PhC waveguide without the need to model the propagation in the rest of the sample, in contrast to the case when only regular transmission spectra are available.

As a model system for our experiment, we use a five component sample (Figure 1a). There are two polymer access

Received: July 17, 2013
Revised: November 1, 2013

   dx.doi.org/10.1021/nl4026456 | *Nano Lett.* XXXX, XXX, XXX−XXX

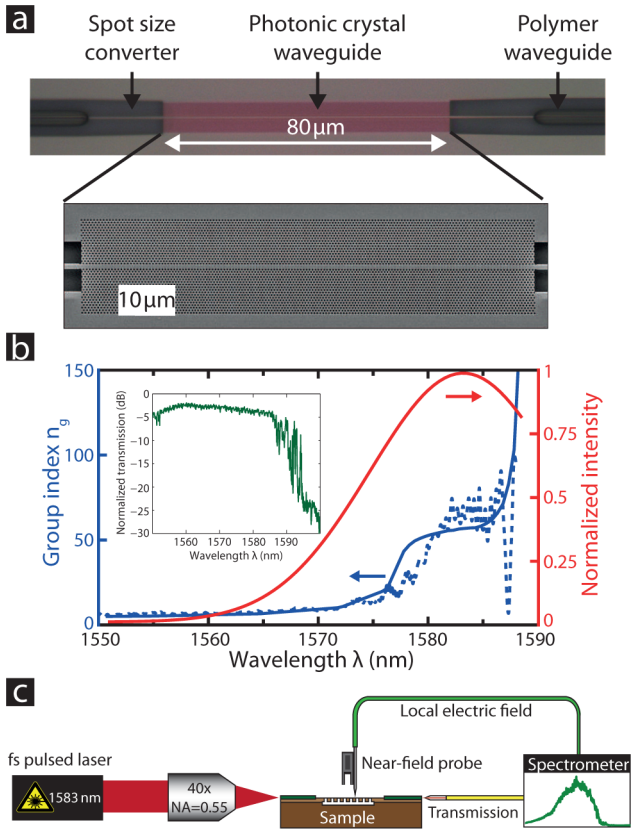

Figure 1. Sample and setup. (a) Optical microscope picture of the central part of the photonic sample. The PhC waveguide is visible in the middle. At the sides, the silicon spot-size converters and part of the polymer access waveguides can be seen. The inset shows a scanning electron micrograph of the silicon PhC. (b) The measured (dashed) and calculated (solid) group index distribution as a function of wavelength (blue, left axes) and the spectral density of the laser coupled into the sample (red, right axis). The inset shows the measured linear transmission of the PhC waveguide normalized to the transmission of a SU8 polymer waveguide. (c) Schematic of our experimental setup.

waveguides, one for each facet, and the silicon PhC that is connected to the access waveguides with two silicon spot-size converters. The polymer waveguides consist of SU-8 photoresist, are a few millimeters long, and have a large cross-section, a width and a height of roughly 5 and 2 μm, respectively, to enhance the efficiency of the light incoupling.[31] Each spot-size converter is a 50 μm long inverse taper, whose purpose is to funnel the light from the polymer access waveguides to the PhC waveguide. The photonic crystal waveguide has a length of 80 μm and is therefore at least 10 times shorter than each of the access polymer waveguides. Details about the design and the fabrication of the PhC waveguide can be found in the Supporting Information.

We measure the group index n_g characteristics by means of Fourier transform spectral interferometry.[32] The result, presented in Figure 1b, indicates that there is a plateau of $n_g \sim 60$ between 1577 and 1587 nm. The group index diverges for longer wavelength as the cutoff is approached. For wavelengths shorter than 1577 nm, the group index tends to a value of 5. We also calculate the dispersion relation of the slow light PhC waveguide using MIT Photonics Band (MPB) package.[33] The extracted group index is in good agreement with the MPB calculation (dashed and solid blue curve in Figure 1b, respectively), indicating the high quality of fabrication and characterization of the sample.

Finally, we also characterize the linear response of our sample by measuring transmission at low intensities (inset in Figure 1b). Up to a wavelength of 1587 nm the transmission is basically flat at −5 dB. For longer wavelength, the transmission drops rapidly, up to −30 dB at 1600 nm, due to the slowdown of the guided mode, which increases the backscattering and the out-of-plane scattering[34] and the approaching cutoff. The contribution of the linear material absorption to this loss is negligible since single photons at telecom wavelengths do not possess enough energy to bridge the electronic band gap.

As shown in Figure 1c, we end-fire couple femtosecond pulses centered at 1583 nm, which are generated by an optical parametric oscillator (Spectra Physics OPAL) into our sample using a 40x aspheric lens (NA = 0.55). At the end facet of the sample, a lensed fiber collects the transmitted light, which is then spectrally analyzed. The laser delivers bandwidth-limited pulses of a temporal length of 180 fs and a concomitant intensity bandwidth of 20 nm (fwhm). To investigate nonlinear optical effects the laser power coupled into the sample can be varied by a neutral density filter. The values of the input power mentioned in this Letter are all determined before the incoupling lens. A maximum limit for the input power of 26 mW is chosen for all experiments to avoid damage to our sample, which was found to occur at ∼30mW.

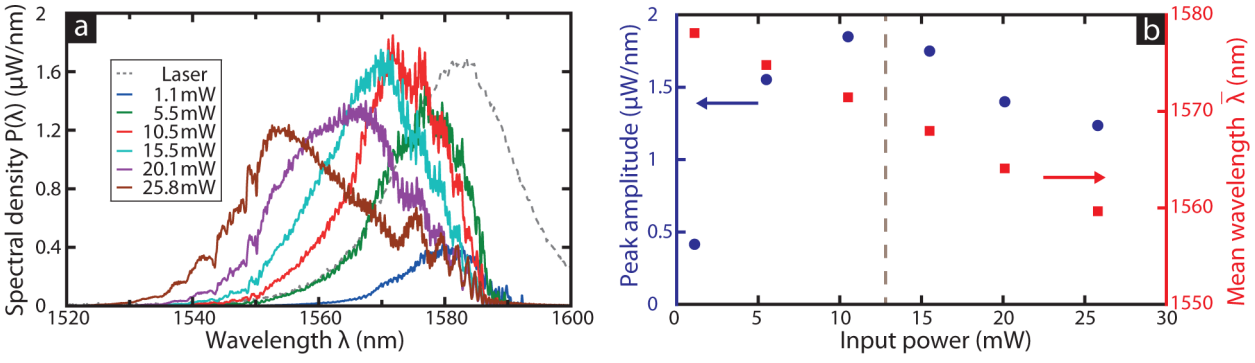

Figure 2. Spectral transmission measurements of the whole sample. (a) Transmission spectra for different average input powers and the spectrum of the laser before the sample, for comparison. (b) The dependence of the peak amplitude and the mean wavelength of the transmission spectra on the input power. The gray dashed line marks the boundary between the regions where the peak amplitude increases, and where it decreases with input power.

dx.doi.org/10.1021/nl4026456 | Nano Lett. XXXX, XXX, XXX−XXX

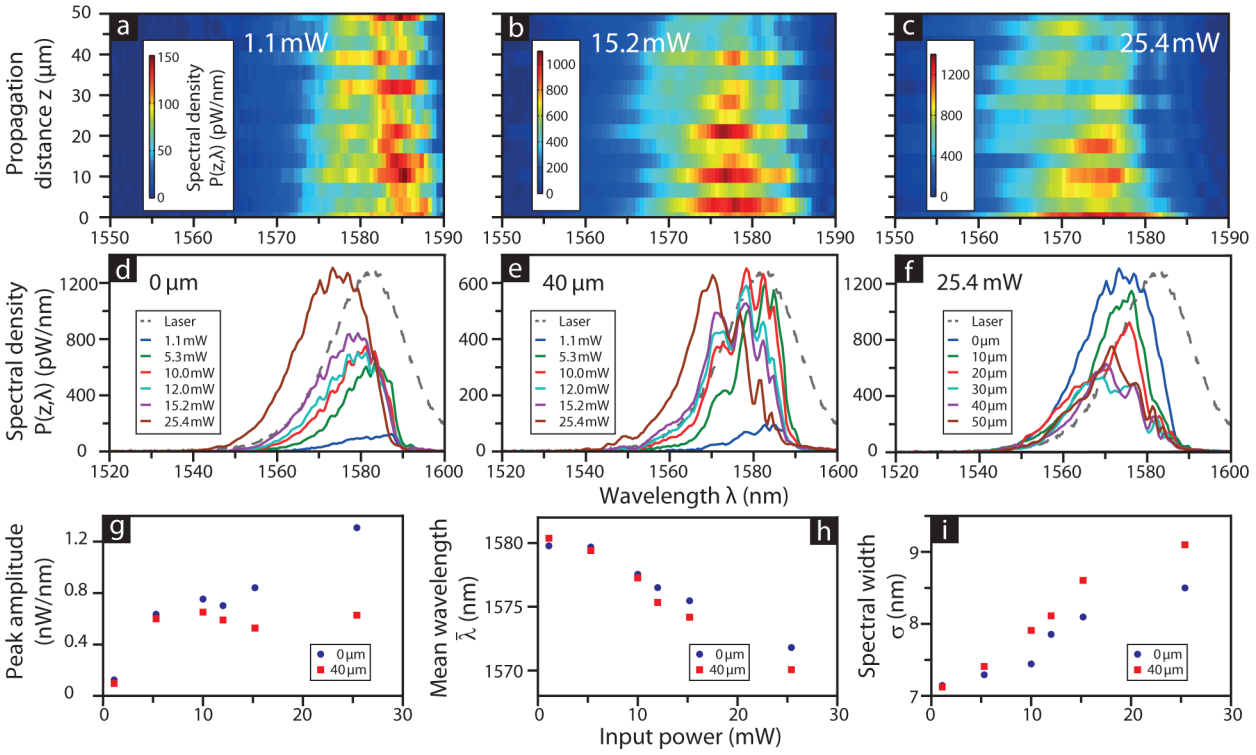

Figure 3. Spectrally resolved near-field measurements along the PhC waveguide. Three near-field measurement series showing the evolution of the spectral density of the pulse for average input powers of (a) 1.1, (b) 15.2, and (c) 25.4 mW. A series of spectra taken at the beginning (d) and after 40 μm propagation (e) in the slow light PhC waveguide for different average input powers. (f) A series of spectra taken in 10 μm steps at an average input power of 25.4 mW. Additionally, the laser spectrum is included in (d–f). Peak amplitude (g), mean wavelength (h), and spectral width (i) of the spectra series shown in (d,e).

Near-field measurements are performed by means of a home-built NSOM. By placing the near-field probe at different locations on the sample and spectrally analyzing the detected light, the evolution of the spectral density can be tracked. At each point the spectrum is collected while scanning the near-field probe transversally over the waveguide in order to average out the complex lateral field distribution of the PhC Bloch modes.[35] Note that the resolution is limited by the aperture size, which is in our case ~250 nm. In principle, the resolution could be pushed further into the nanoscale by decreasing the aperture size at the cost of less collected light.

First, transmission measurements are performed to characterize the nonlinear response of the complete sample. Figure 2a shows spectra measured for six different average input powers ranging from 1.1 to 25.8 mW. The dependence of the shape of the transmitted spectrum on the input power is a clear signature of the presence of nonlinear effects.[18] The most obvious feature is that the peak amplitude does not scale linearly with the input power as shown in Figure 2b. The maximum value of the spectrum increases until 10.5 mW. For higher input powers the peak amplitude declines.

The second feature that can be observed is a blueshift of the spectral density $P(\lambda)$, which we quantify by calculating the mean wavelength $\bar{\lambda}$ of each spectrum

$$\bar{\lambda} = \frac{\int \lambda P(\lambda) d\lambda}{\int P(\lambda) d\lambda} \quad (1)$$

Figure 2b depicts the dependence of $\bar{\lambda}$ on input power. It is clear that the mean wavelength blueshifts at higher powers. In the linear optical regime, we expect to observe a transmission spectrum resembling that of the input laser but cut off around 1587 nm. This spectral reshaping, which is indeed observed for low input power, is due to the increased linear scattering loss at longer wavelengths and the approaching cutoff. However, for increasing input power the spectrum changes in shape. In addition to the observed blueshift at higher input powers, the spectral density broadens (a quantified measure of this broadening can be found in the Supporting Information). We note that the broadening and blueshift cannot be due to the linear scattering loss in the PhC waveguide, as these changes occur mostly at wavelengths below 1585 nm, where this linear loss is constant (inset in Figure 1b). In summary, the power dependence of the transmission spectra is clearly indicative of nonlinear pulse propagation.

The transmission spectra represent the response of the complete composite sample. The question that now arises is which of the observed spectral changes occur in the PhC waveguide and which are due to the other four components of our sample. In order to answer this question, we perform in situ NSOM measurements of the pulse propagating inside the photonic crystal waveguide. Each of the measurements, presented in Figure 3a–c, consists of 19 spectra collected at positions evenly distributed over a distance of 50 μm along the PhC for the different input powers. These measurements show that we can determine the spectra of the propagating pulse as a function of position and thereby gain access to its spectral evolution at the nanoscale.

For all input powers, we observe various abrupt amplitude changes between the spectra taken at successive propagation distances. This modulation in the amplitude is an artifact caused by the Bloch nature of the photonic modes in the

dx.doi.org/10.1021/nl4026456 | Nano Lett. XXXX, XXX, XXX–XXX

waveguide. That is, the locally measured electric field amplitude is strongly dependent on the exact position of the probe within a single unit cell[24] and the positional accuracy is mainly limited by the thermal drift and the size of the investigated area of several tens of μm^2. However, the shape of the spectral density does not depend on the probe position within a unit cell. While it is tempting to normalize the data, in doing so we would lose any information about a possible amplitude drop due to absorption and so we analyze the unnormalized spectra.

Beside these abrupt amplitude variations there is no significant drop in amplitude of the spectral density with propagation visible for an input power of 1.1 mW (cf. Figure 3a). That is, there is no significant absorption occurring inside the PhC waveguide at this low input power. From this and the fact the shape of the spectrum of the pulse is the same throughout the waveguide, we conclude that nonlinear effects are negligible here. At 15.2 mW the evolution of the spectral density starts to show evidence of nonlinear effects (cf. Figure 3b), since the peak amplitude decays by 50% in the first 50 μm. For the highest investigated input power, close to the damage threshold, shown in Figure 3c, the amplitude decay of the spectral density occurs even faster. The peak amplitude of the spectral density decreases by 50% in the first 30 μm. Thus, this series of spectra demonstrate that the pulse experiences power-dependent losses during propagation inside the PhC waveguide.

Interestingly, we observe a power dependence of the spectral density at the beginning of the PhC waveguide. For example, a blueshift due to increased input power becomes obvious by comparing these spectra to the input laser spectrum (Figure 3d). To quantify the spectral changes that occurred before the PhC, we investigate a series of spectra taken at the start of the PhC for different input powers, shown in Figure 3d. There are four different features that can be analyzed: shape, peak amplitude, mean wavelength, and spectral width. First, the shape of spectra at the input of the PhC remains the same for all input powers, that is, a Gaussian cutoff at longer wavelength. Second, the peak amplitude of the spectra does not scale linearly with input power (cf. blue dots in Figure 3g). Third, there is a power-dependent blueshift of the spectral density. This wavelength shift can be quantified using eq 1. As shown in Figure 3h, a change of the input power from 1.1 to 25.4 mW results in a blueshift of 8 nm. Fourth, the spectra broaden slightly with input power, that is, the spectral width (defined in the Supporting Information) increases by ~1.5 nm between the spectra measured at 1.1 and 25.4 mW (cf. blue dots in Figure 3i). These observations suggest that the intensity of the pulse is sufficiently high for nonlinear effects to play a role in the access waveguide or the silicon inverse taper.

To quantify the effect of the PhC waveguide on the changes in the laser spectrum, we measure a series of spectra after 40 μm propagation inside the slow light photonic crystal waveguide (Figure 3e) for the same range of input powers. A comparison of Figure 3d,e makes it obvious that the shape of the spectral density changes significantly with input power. Note that after 40 μm inside the PhC, the spectra measured by NSOM begin to resemble those measured in transmission (Figure 2a). Hence, this observation together with the fact that the shape of the spectra at the beginning of the PhC is not power-dependent, shows that the reshaping of the spectral density happens inside the PhC waveguide.

The peak amplitude of the spectra at 40 μm also scales in a nonlinear fashion with input power but in a more drastic fashion than at the beginning of the PhC waveguide as shown in Figure 3g. At 10 mW, the peak amplitude reaches its maximum value after which it shows a small drop until finally recovering for 25.4 mW. This scaling of the peak amplitude shows qualitative agreement with the trend observed in the transmission spectra (Figure 2 b) other than at the highest input power.

In addition, a power-dependent blueshift can be again observed near the end of the PhC (cf. blue squares in Figure 3h). At an input power of 1.1 mW the spectrum has a mean wavelength of 1580 nm that decreases to a value of 1570 nm when the input power is increased to 25.4 mW. Interestingly, this wavelength shift of 10 nm is only slightly larger than the shift observed at the beginning of the PhC waveguide. Moreover, since the transmission spectra exhibit a blueshift roughly twice as large, this suggests that most of the shift in wavelength of the spectral density occurs in the other components of the sample.

A similar observation can be made for the spectral broadening presented in Figure 3i. By comparing the spectral width of the two measurement series we conclude that only a small fraction of the spectral broadening occurs inside the PhC waveguide. The transmission spectra show a broadening of 5 nm (cf. Supporting Information) which is three times larger than the broadening observed in the PhC. Thus, together with the blueshift the broadening of the spectral density occurs mainly in the other components of the sample, and not in the PhC waveguide. This may seem unexpected, particularly given the slow-light enhancement and the spatial confinement of the light in the PhC, yet it can be explained with two reasons. First, the pulse is temporally broadened due to dispersion before it enters the photonic crystal waveguide giving rise to a decreased peak amplitude. Second, the blueshift of the spectral density already before the photonic crystal waveguide causes the pulse to experience smaller group indices than would be a priori assumed. In conclusion, the slow light photonic crystal waveguide has a major effect on the reshaping and the scaling of the peak amplitude, but the blueshift and the broadening of the spectral density occurs mainly in the other components of the sample.

There remains the question about the cause of the spectral reshaping. To answer it we investigate the evolution of the spectral density inside the PhC waveguide at an input power of 25.4 mW by comparing spectra at different locations. This is shown in Figure 3f for six spectra, taken in 10 μm steps. This measurement suggests that there is no energy redistribution inside the spectrum, for example, energy transfer from the long wavelengths to the shorter ones, since the spectral density taken at the beginning of the PhC waveguide possesses the highest amplitude at each wavelength. Instead it seems more that the spectral reshaping originates from different decay behavior of different spectral components, that is, an increased amplitude drop at the long wavelength side.

In essence, the near-field measurements allow us to separate the spectral reshaping happening inside different devices of an integrated photonic circuit on the nanoscale that is not possible by means of transmission measurements. Additionally, the NSOM measurements show that although the polymer waveguides are at least one magnitude longer than the PhC waveguide, most of the spectral reshaping occurs inside the PhC. This observation confirms the potential of slow light for enhancing nonlinear optics.

dx.doi.org/10.1021/nl4026456 | Nano Lett. XXXX, XXX, XXX−XXX

To gain more insight into the physical processes playing a role in the reshaping of the spectral density we model pulse propagation by means of the nonlinear Schrödinger equation (NLSE),[36] which includes dispersion, various nonlinear optical effects and free-carrier dynamics. Because the spectrum of our pulse covers a broad range of different group indices we take the full dispersion relation $\gamma(\omega)$ of the PhC waveguide into account. Therefore, we split the NLSE into two equations, one that deals with the nonlinear optical effects and the free-carrier dynamics, and one that considers the dispersion. Concurrently, we solve an auxiliary rate equation describing the temporal evolution of the free-carrier density.[37]

The first equation, which describes nonlinear and free-carriers effects during propagation, is most conveniently formulated in the time domain

$$\frac{\partial A}{\partial z} = -\frac{\alpha}{2}A + \left(-\frac{\beta}{2A_{\text{eff}}} + i\frac{2\pi}{\lambda A_{\text{eff}}}n_2\right)|A|^2 A - \left(\frac{\sigma}{2} + i\frac{2\pi}{\lambda}k_c\right)N_c A \quad (2)$$

The meaning and the value of the parameters in eq 2 and subsequent equations, which are either material- or geometry-dependent and therefore taken from literature, can be found in Table 1.

Table 1. The Names and Values of the Parameters Used in the Numerical Calculations and the References from Which They Were Taken[a]

parameter	name	value	slowdown scaling	reference
A_{eff}	effective mode area	0.66 μm^2		
α	linear loss coefficient	20 dB/cm	S	38
β	TPA coefficient	1 cm/GW	S^2	39
n_2	Kerr coefficient	6×10^{-14} cm^2/W	S^2	39
σ	FCA cross-section	1.45×10^{-21} m^2	S	40
k_c	FCD coefficient	1.35×10^{-27} m^3	S	41
τ_{rec}	free-carrier recombination time	450 ps		1

[a]The effective mode area was extracted from MPB simulations and the slowdown scaling factor for each parameter is given, if applicable. The linear loss coefficient α accounts only for scattering loss and its dependence on the slowdown is explained in more detail in the Supporting Information.

Equation 2 describes how the slowly varying temporal envelope $A(z,t)$ of the pulse, defined by $A(z,t) = (I(z,t)\cdot A_{\text{eff}})^{1/2}$, where $I(z,t)$ is pulse intensity, is influenced by third-order nonlinear effects, that is, two-photon absorption (TPA) and self-phase modulation (SPM) due to the Kerr effect, and by free-carriers dynamics, that is, free-carrier absorption (FCA) and free-carrier dispersion (FCD).

The temporal evolution of the free-carrier density $N_c(t)$ is governed by the following rate equation[38]

$$\frac{dN_c}{dt} = \frac{\pi\beta}{h\omega_0 A_{\text{eff}}^2}|A|^4 - \frac{N_c}{\tau_{\text{rec}}} \quad (3)$$

where h is the Planck constant and ω_0 the central angular frequency of the pulse. In this equation, we see that free-carriers are only created by two-photon absorption (first term) and that they recombine with a lifetime τ_{rec} (second term). The free-carrier lifetime has a value of a few hundred picoseconds in silicon structures featuring a large surface area.[1] Since the laser pulse needs less than 16 ps to propagate through the PhC waveguide, the amount of carrier recombination during pulse propagation is negligible. Moreover, free-carrier accumulation between pulses is disregarded since the time between subsequent laser pulses is 12.5 ns and therefore much longer than the carrier lifetime.

In contrast to the nonlinear effects and the free-carrier dynamics that are dealt with in the time domain, it is more beneficial to treat dispersion in the frequency domain. Here the temporal broadening of the pulse envelope can be described as a simple differential equation for the spectral density $\hat{A}(z)$, which is the temporal Fourier transform of $A(z,t)$:

$$\frac{\partial \hat{A}}{\partial z} = i\gamma(\omega - \omega_0)\hat{A} \quad (4)$$

Details of how the system of equations is solved and fitted to our experimental data can be found in the Supporting Information.

In addition, it is important to take the slow group velocity of the light inside the PhC waveguide into account, because it has been shown that slow light propagation enhances nonlinear effects as well as interactions of the pulse with free carriers.[38] Two-photon absorption and the Kerr effect, which leads to self-phase modulation, scale quadratically with the so-called slowdown factor S which is defined by $S = n_g/n_{si}$.[42] This quadratic enhancement arises because[43] (I) a slower pulse has more time to interact with matter, and (II) the pulse is spatially compressed upon entering into the slow light waveguide, leading to an increase in its intensity. In contrast, effects which are not influenced by the pulse intensity, that is, linear loss, free-carrier absorption, and free-carrier dispersion scale only linearly with S. Thus, the material parameters describing these effects are replaced by effective parameters to emulate the slow light enhancement. These effective parameters consist of the values listed in Table 1, properly scaled with the slowdown factor. Further, we note that the effective mode area A_{eff} is related to the group index in a nontrivial fashion. However, for most of the spectral regime in our experiment the variation of A_{eff} is minor. Thus, the effective mode area is taken to be constant in our simulations.

It is crucial to account for the frequency dependence of the slowdown factor S, which is mimicked by solving our model several times, once per investigated wavelength, and taking the group index valid at that wavelength into account for the slow light enhancement. Thus, for the sake of simplicity our approach inherently assumes that S is constant and we only investigate how one specific spectral component evolves with propagation. If we wanted to investigate the evolution of the complete spectrum of the pulse, we would have to slice the spectral density and calculate the evolution of these slices by solving the model repeatedly. To minimize the computation effort and still show that this approach delivers accurate results, we investigate only three different wavelengths, namely 1565, 1575, and 1580 nm, which feature different group indices with values of 7, 18 and 53, respectively.

Figure 4 presents a comparison between typical modeling results and data taken from the near-field measurements (Figure 3c). The figure shows how the three spectral components decay with propagation inside the PhC waveguide.

dx.doi.org/10.1021/nl4026456 | Nano Lett. XXXX, XXX, XXX−XXX

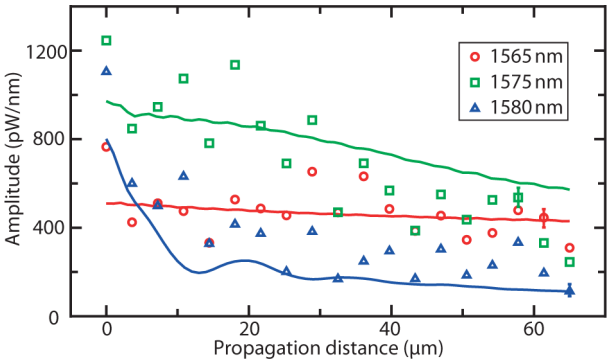

Figure 4. Decay behavior of different spectral components during propagation inside the PhC waveguide. The experimentally (points) and theoretically (solid curves) determined spectral amplitude as a function of propagation distance at three different wavelengths. The experimental data is taken from Figure 3c where the average input power is 25.4 mW. For each wavelength an error bar is depicted on the right side of the figure.

Clearly, the longest wavelength experiences the fastest amplitude decay. In contrast, the amplitude of the shortest wavelength stays constant. Thus, we find an excellent quantitative agreement between the modeling and the experimental results for all spectral components considered, using material parameters found in literature. Only the decay for the wavelength of 1575 nm seems to be slightly underestimated, suggesting that some of the optical properties (e.g., TPA or linear loss coefficient) of our sample differ from those reported in the literature. This observation illustrates the potential of our method to investigate the local effective optical properties inside an integrated photonic circuit. Over the small wavelength range that our pulses span the material parameters of the PhC are practically constant while the group index varies greatly (cf. Figure 1b). Hence, different wavelengths of light within the PhC experience vastly different slowdown factors, and it is this dispersion of the slow light enhancement that causes the observed spectral density reshaping.

The oscillations visible in the experimental data originate from the positioning uncertainty of the probe inside the photonic crystal waveguide unit cell mentioned before. Consequently, the error bars represent the standard variation of the intensity distribution of the guided mode inside a unit cell of the PhC, except for the longest wavelength where a 5% noise level is assumed. In the slow light regime, the light will be more sensitive to many different effects, which therefore justifies a larger error bar than the spatial mode profile would suggest. Details about the calculation of the error bars can be found in the Supporting Information.

We now turn to discuss the influence of the different physical effects that occur during the pulse propagation, which can be separated in two categories: (I) those that lead to losses and (II) those that change the shape of the spectrum. There are three processes that may lead to an amplitude decay with propagation, scattering, TPA, and FCA. The linear losses due to scattering are too small to have a significant impact over a 50 μm distance which we also observe in our measurements, since there is no absorption visible at the lowest input power (cf. Figure 3a). Thus, the measured amplitude decay is mainly caused by TPA and FCA.

SPM and FCD are usually considered to be the source for spectral reshaping such as a blueshift.[40] However, in our experiment both processes do not have a significant influence on the spectral shape, as shown in Figure 3f. Instead, the reshaping is caused by dispersion of the PhC waveguide, which in general has a 3-fold influence. First, a large dispersion stretches the pulse temporally and therefore limiting its peak intensity. Second, a wavelength dependence of the effective material parameters as discussed above is created. Third, it also causes a wavelength dependence of the free-carrier effects leading to an enhanced decay of the slower propagating spectral components, that is, longer wavelengths. This is explained by the build-up of the free-carrier density in time between the rising and trailing edge of a single pulse so that the trailing edge, containing longer wavelengths, will experience enhanced FCA and FCD.[44] In essence, the spectral reshaping stems from the wavelength-dependent slowdown factor S and an interplay of dispersion and the temporal dynamics of the free carriers.

Next, we demonstrate that a similar approach, which uses the transmission spectra from the entire composite sample (cf. Figure 2), does not accurately predict the spectral evolution in the PhC waveguide. We again solve eqs 2−4 using the same parameter values and assume that there are no nonlinear effects inside the polymer access waveguide and spot-size converter. Only the temporal broadening that occurs before the PhC waveguide is taken into account.

We try to model the evolution with input power of the same three wavelengths as above and compare it with experimental data taken from the transmission measurements, as shown in Figure 5. There is a clear discrepancy between the model and

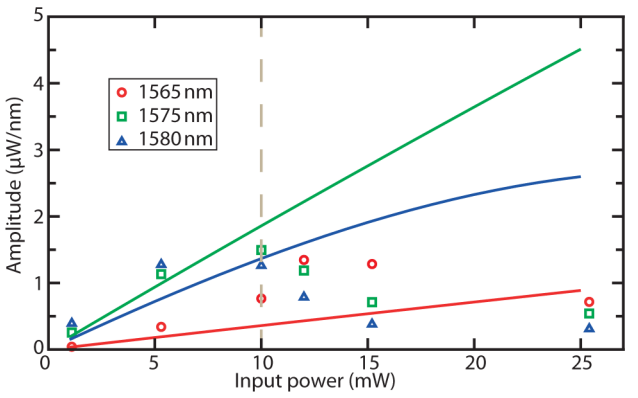

Figure 5. Scaling behavior of different wavelengths with power in the transmission spectra. The experimentally (points) and theoretically (solid curves) determined spectral amplitude as a function of average input power for three different wavelengths. The experimental data is taken from Figure 2a. The gray dotted line marks the input power from which on the evolution of the spectral density differs significantly.

the experiment. First, the model no longer reproduces the scaling of the amplitudes with input power. The measured amplitudes of all spectral components show a decrease with input power for very high input powers, whereas the modeling results feature a steady increase. Second, the blueshift visible in the measurement is not reproduced by the model. In the measured data, at the lowest input powers the longest wavelength exhibits the highest amplitude, whereas for high input powers the shortest wavelength has the highest amplitude, while the model does not exhibit this behavior. Hence, the model can reproduce neither the peak amplitude scaling nor the power-dependent spectral reshaping visible in the transmission measurements.

dx.doi.org/10.1021/nl4026456 | Nano Lett. XXXX, XXX, XXX−XXX

Overall, it seems that the discrepancy between our transmission measurements and the model can be explained by a power-dependent absorption process, which is missing or underestimated in the modeling approach at higher input powers. We understand this discrepancy in terms of the blueshift that occurs before the PhC waveguide. The blueshift transfers energy to a spectral region with higher dispersion, so that the spectral density covers a larger range of group indices. This leads to a dramatic enhancement of the reshaping, as explained above, for increasing input power.

This interpretation is also supported by our experimental observations. For input powers higher than 15.2 mW, we observed a change in the spectral reshaping in the transmission spectra (Figure 2a) as well as in the near-field measurements (Figure 3e). The measured spectral density is no longer centered on the flat dispersion band at 1580 nm, but shifted toward 1570 nm, where the group index changes significantly with wavelength. Thus, the strong reshaping goes hand in hand with and is actually influenced by the blueshift in front of the PhC waveguide. In essence, the failure of the model to reproduce the evolution of the transmission spectra of the composite structure shows that obtaining the nonlinear optical behavior of the PhC waveguide that is part of a composite structure is far from trivial, since the other components may have a significant influence.

In conclusion, we presented a near-field scanning optical microscopy technique that can be used to test and evaluate nonlinear pulse propagation inside single components of integrated photonic circuits on the nanoscale in analogy to the wafer testing applied in the electronic industry. This approach allowed us to gain information about the evolution of the spectral density inside the composite sample and to unravel the different physical occurring during ultrashort propagation. Specifically, the observed spectral reshaping is mainly caused by nonlinear optical effects inside a slow light photonic crystal waveguide and can be understood by an interplay between dispersion, free-carrier effects, and a wavelength-dependent slow light enhancement of various nonlinear effects. Reaching the same insight with only conventional transmission measurements, which reflect the behavior of the complete sample, is far from trivial, since the characteristics of the different components influence each other in a complex manner in the nonlinear optical regime.

■ ASSOCIATED CONTENT

Supporting Information

More details about sample design and fabrication, broadening of the transmission spectra, numerical calculations as well as error bars. This material is available free of charge via the Internet at http://pubs.acs.org.

■ AUTHOR INFORMATION

Corresponding Author

*E-mail: wulf@amolf.nl.

Notes

The authors declare no competing financial interest.

■ ACKNOWLEDGMENTS

We thank Hinco Schoenmaker for technical support. We thank Isabella H. Rey and Thomas F. Krauss for providing the photonic crystal waveguide and the linear transmission measurements. This work is part of the research programme of the Foundation for Fundamental Research on Matter (FOM), which is part of The Netherlands Organisation for Scientific Research (NWO). The work is also supported by the European Union (Project SPANGL4Q) and NanoNextNL, a micro- and nanotechnology consortium of the Government of The Netherlands and 130 partners.

■ REFERENCES

(1) Almeida, V. R.; Barrios, C. A.; Panepucci, R. R.; Lipson, M. *Nature* **2004**, *431*, 1081−1084.

(2) Koos, C.; Vorreau, P.; Vallaitis, T.; Dumon, P.; Bogaerts, W.; Baets, R.; Esembeson, B.; Biaggio, I.; Michinobu, T.; Diederich, F.; Freude, W.; Leuthold, J. *Nat. Photonics* **2009**, *3*, 216−219.

(3) Xia, F.; Sekaric, L.; Vlasov, Y. A. *Nat. Photonics* **2007**, *1*, 65−71.

(4) Beggs, D. M.; Rey, I. H.; Kampfrath, T.; Rotenberg, N.; Kuipers, L.; Krauss, T. F. *Phys. Rev. Lett.* **2012**, *108*, 213901.

(5) Vlasov, Y. A.; O'Boyle, M.; Hamann, H. F.; McNab, S. J. *Nature* **2005**, *438*, 65−69.

(6) Foster, M. A.; Turner, A. C.; Sharping, J. E.; Schmidt, B. S.; Lipson, M.; Gaeta, A. L. *Nature* **2006**, *441*, 960−963.

(7) Salem, R.; Foster, M. A.; Turner, A. C.; F.Geraghty, D.; Lipson, M.; Gaeta, A. L. *Nat. Photonics* **2008**, *2*, 35−38.

(8) Johnson, S. G.; Villeneuve, P. R.; Fan, S.; Joannopoulos, J. D. *Phys. Rev. B* **2000**, *62*, 8212−8222.

(9) *Roadmap on Photonic Crystals*; Noda, S., Baba, T., Eds.; Kluwer Academic Press: New York, 2003.

(10) Li, J.; White, T. P.; O'Faolain, L.; Gomez-Iglesias, A.; Krauss, T. F. *Opt. Express* **2008**, *16*, 6227−6232.

(11) Petrov, A. Y.; Eich, M. *Appl. Phys. Lett.* **2004**, *85*, 4866−4868.

(12) Baba, T. *Nat. Photonics* **2008**, *2*, 465−473.

(13) Corcoran, B.; Monat, C.; Grillet, C.; Moss, D. J.; Eggleton, B. J.; White, T. P.; O'Faolain, L.; Krauss, T. F. *Nat. Photonics* **2009**, *3*, 206−210.

(14) Inoue, K.; Oda, H.; Ikeda, N.; Asakawa, K. *Opt. Express* **2009**, *17*, 7206−7216.

(15) McMillan, J. F.; Yu, M.; Kwong, D.-L.; Wong, C. W. *Opt. Express* **2010**, *18*, 15484−15497.

(16) Boyd, R. W. *Nonlinear Optics*; Academic Press: New York, 2008.

(17) Boyraz, O.; Indukuri, T.; Jalali, B. *Opt. Express* **2004**, *12*, 829−834.

(18) Rieger, G. W.; Virk, K. S.; Young, J. F. *Appl. Phys. Lett.* **2004**, *84*, 900−902.

(19) Hsieh, I.-W.; Chen, X.; Liu, X.; Dadap, J. I.; Panoiu, N. C.; Chou, C.-Y.; Xia, F.; Green, W. M.; Vlasov, Y. A.; Osgood, R. M. *Opt. Express* **2007**, *15*, 15242−15249.

(20) Husko, C.; Combrié, S.; Tran, Q. V.; Raineri, F.; Wong, C. W.; Rossi, A. D. *Opt. Express* **2009**, *17*, 22442−22451.

(21) Roberts, G.; Taenzler, F.; Burns, M. *An Introduction to Mixed-Signal IC Test and Measurement*; Oxford University Press: New York, 2011.

(22) Betzig, E.; Trautman, J. K.; Harris, T. D.; Weiner, J. S.; Kostelak, R. L. *Science* **1991**, *251*, 1468−1470.

(23) Volkov, V. S.; Bozhevolnyi, S. I.; Borel, P. I.; Frandsen, L. H.; Kristensen, M. *Phys. Rev. B* **2005**, *72*, 035118.

(24) Burresi, M.; Engelen, R. J. P.; Opheij, A.; van Oosten, D.; Mori, D.; Baba, T.; Kuipers, L. *Phys. Rev. Lett.* **2009**, *102*, 033902.

(25) Balistreri, M. L. M.; Gersen, H.; Korterik, J. P.; Kuipers, L.; van Hulst, N. F. *Science* **2001**, *294*, 1080−1082.

(26) Abashin, M.; Ikeda, K.; Saperstein, R.; Fainman, Y. *Opt. Lett.* **2009**, *34*, 1327−1329.

(27) Trägårdh, J.; Gersen, H. *Opt. Express* **2013**, *21*, 16629−16638.

(28) Nagahara, T.; Imura, K.; Okamoto, H. *Rev. Sci. Instrum.* **2004**, *75*, 4528−4533.

(29) Richter, A.; Behme, G.; Süptitz, M.; Lienau, C.; Elsaesser, T.; Ramsteiner, M.; Nötzel, R.; Ploog, K. H. *Phys. Rev. Lett.* **1997**, *79*, 2145−2148.

(30) Louvion, N.; Gérard, D.; Mouette, J.; de Fornel, F.; Seassal, C.; Letartre, X.; Rahmani, A.; Callard, S. *Phys. Rev. Lett.* **2005**, *94*, 113907.

(31) McNab, S.; Moll, N.; Vlasov, Y. *Opt. Express* **2003**, *11*, 2927–2939.
(32) Gomez-Iglesias, A.; O'Brien, D.; O'Faolain, L.; Miller, A.; Krauss, T. F. *Appl. Phys. Lett.* **2007**, *90*, 261107.
(33) Johnson, S.; Joannopoulos, J. *Opt. Express* **2001**, *8*, 173–190.
(34) Hughes, S.; Ramunno, L.; Young, J. F.; Sipe, J. E. *Phys. Rev. Lett.* **2005**, *94*, 033903.
(35) Gersen, H.; Karle, T. J.; Engelen, R. J. P.; Bogaerts, W.; Korterik, J. P.; van Hulst, N. F.; Krauss, T. F.; Kuipers, L. *Phys. Rev. Lett.* **2005**, *94*, 123901.
(36) Agrawal, G. P. *Nonlinear Fiber Optics*; Academic Press: New York, 2001.
(37) Dekker, R.; Usechak, N.; Föst, M.; Driessen, A. *J. Phys. D: Appl. Phys.* **2007**, *40*, R249–R271.
(38) Monat, C.; Corcoran, B.; Ebnali-Heidari, M.; Grillet, C.; Eggleton, B. J.; White, T. P.; O'Faolain, L.; Krauss, T. F. *Opt. Express* **2009**, *17*, 2944–2953.
(39) Dinu, M.; Quochi, F; Garcia, H. *Appl. Phys. Lett.* **2003**, *82*, 2954–2965.
(40) Yin, L.; Agrawal, G. P. *Opt. Lett.* **2007**, *32*, 2031–2033.
(41) Xu, Q.; Lipson, M *Opt. Lett.* **2006**, *31*, 341–343.
(42) Soljačić, M.; Joannopoulos, J. D. *Nat. Mater.* **2004**, *3*, 211–219.
(43) Bhat, N. A. R.; Sipe, J. E. *Phys. Rev. E* **2001**, *64*, 056604.
(44) Corcoran, B.; Monat, C.; Pudo, D.; Eggleton, B. J.; Krauss, T. F.; Moss, D. J.; O'Faolain, L.; Pelusi, M.; White, T. P. *Opt. Lett.* **2010**, *35*, 1073–1075.

Supporting Information for Unravelling nonlinear spectral evolution using nanoscale photonic near-field point-to-point measurements

Matthias Wulf,* Daryl M. Beggs, Nir Rotenberg, and L. Kuipers

Center for Nanophotonics, FOM Institute for Atomic and Molecular Physics (AMOLF), Science Park 104, 1098XG, Amsterdam, The Netherlands

E-mail: wulf@amolf.nl

Sample details

The photonic crystal (PhC) consists of a 220 nm thick silicon membrane which is perforated with air holes. The holes have a radius of 0.29a and are periodically arranged in a triangular lattice ($a = 420\,nm$). One row of holes is not present in the $\Gamma - K$ crystal direction, creating the waveguide. The sample was fabricated by electron beam lithography, subsequent dry etching and sacrificial wet etching to release the membrane.[1] The two rows of holes directly adjacent to the waveguide are shifted by -0.11a and 0.06a, respectively, to create a spectral slow light regime with low group velocity dispersion.[2] A negative shift is defined here as a displacement from the position dictated by the triangular lattice towards the waveguide and a positive shift as a displacement away from the waveguide.

The light injection from a ridge waveguide to a slow light photonic crystal can be very inefficient due to an increasing mode mismatch with increasing n_g. In our experiment, this mismatch

*To whom correspondence should be addressed

would result in inefficient in- and outcoupling for wavelengths above 1577 nm. To overcome this problem we have changed the lattice constant of the first and last ten periods of our photonic crystal to a value of 440 nm which shifts the whole bandstructure to longer wavelengths. This shift creates a photonic crystal with $n_g = 5$ across the entire spectrum of our laser, which acts as an interface between the ridge waveguide and the slow light PhC. It has been shown in literature that this gradual approach of first exciting a fast light mode, which then couples to a slow mode, is very efficient and can lead to injection efficiencies above 90 % for group indices up to 100.[3]

Broadening of the transmission spectra

The width of a spectrum can be quantified by calculating its second moment, i.e. variance σ, which is defined by

$$\sigma^2 = \frac{\int (\overline{\lambda} - \lambda)^2 \, P(\lambda) \, d\lambda}{\int P(\lambda) \, d\lambda}. \tag{1}$$

where $\overline{\lambda}$ is the first moment, i.e. mean wavelength, as defined in Eq. (1) in the maintext.

The change of the spectral width, which is the square root of the variance, of the transmission spectra with input power is shown in Supporting Figure 1. It is obvious that the spectra get broader with increasing input power. By going from 1.1 mW to 25.8 mW the spectral width nearly doubles from 7 nm to 12 nm.

Details of the modeling approach

To model the pulse propagation through the PhC waveguide Eq. (2) and Eq. (4) of the maintext are solved by means of the split-step Fourier method.[4] The temporal evolution of free-carrier density N_c is calculated by solving Eq. (3) of the maintext with a first-order finite-difference scheme.[5]

We fit our model to the measured pulse evolution by adjusting only two parameters: a simple scaling factor modeling the near-field probe pickup-efficiency, and a number that describes the

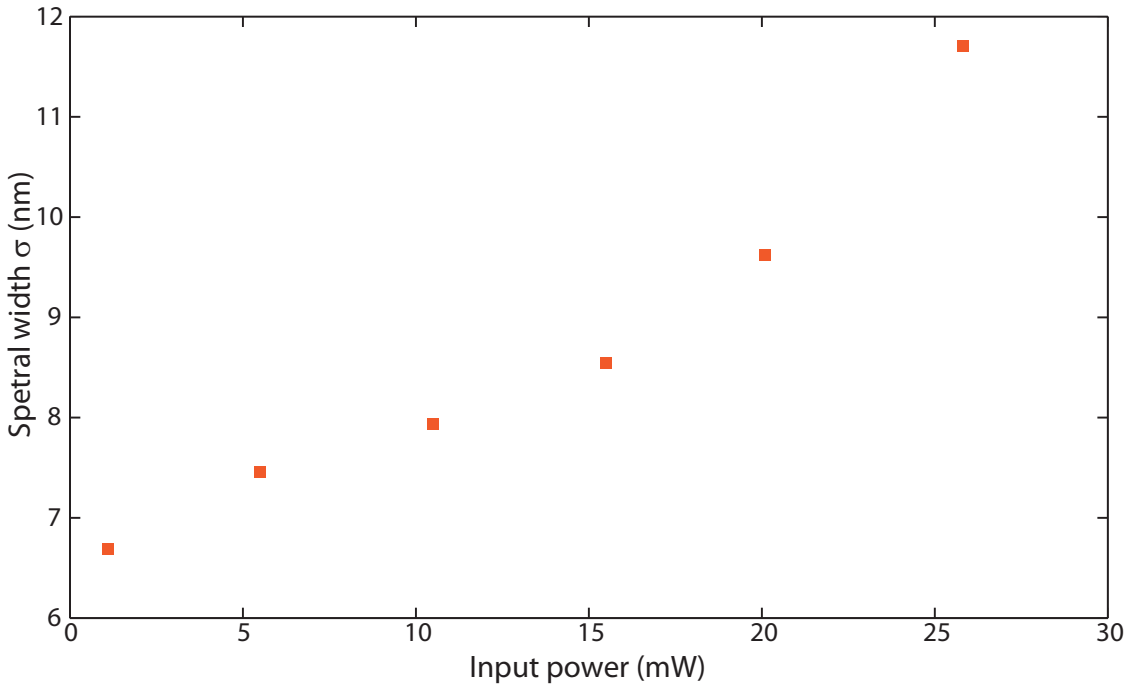

Supporting Figure 1: Spectral width of the transmission spectra shown in figure 2a in the maintext for different average input powers.

chirp the pulse experiences in the polymer access waveguide and the silicon spot-size converter. This latter parameter determines the temporal length of the pulse at the beginning of the PhC waveguide. As starting conditions the first spectrum taken at the beginning of the PhC waveguide and the free-carrier density N_c are set to zero. The best agreement between the model and the experimental results is achieved with a temporal length of 1.38 ps (FWHM). This amount of temporal broadening is reasonable considering the few millimeter distance that the pulse has to propagate through the sample before it enters the PhC waveguide. The blueshift of the spectral density, which occurs either inside the polymer access waveguide or the silicon spot-size converter, is taken into account in the modeling by shifting the centre frequency of the pulse in a one-time fit to the spectrum measured at the beginning of the PhC (cf. Figure 3d of the maintext).

The effective values of all wavelength-dispersive parameters used for simulating the propagation of the different spectral components, shown in Figure 4 of the main text, are presented in Supporting Table 1. The intrinsic material dispersion is negligible over the considered wavelength range. Thus, the observed wavelength dependency arises solely from the photonic crystal induced

dispersion of the slowdown factor S and its influence on the various parameters (see Table 1 in the main text).

The scaling of the linear loss with the slowdown factor is nontrivial, because it consists of both backscattering and out-of-plane scattering, which have different S dependencies. In our modelling we have assumed that the linear losses are dominated by out-of-plane scattering, which is typically for moderate group indices (e.g. $n_g < 50$, depending on the PhC design).[6] Consequently, α_{eff} increases linearly with S.

Supporting Table 1: The effective of all wavelength-dispersive parameters used in the simulation. These values are inclusive of the slowdown enhancement.

Free-space wavelength	$\alpha_{eff}(dB/cm)$	$\beta_{eff}(cm/GW)$	$n_{2,eff}(cm/W)$	$\sigma_{eff}(m^2)$	$k_{c,eff}(m^3)$
1565 nm	22.93	3.97	$2.38 \cdot 10^{-13}$	$2.89 \cdot 10^{-21}$	$2.69 \cdot 10^{-27}$
1575 nm	27.09	26.24	$1.57 \cdot 10^{-12}$	$7.43 \cdot 10^{-21}$	$6.92 \cdot 10^{-27}$
1580 nm	31.78	227.48	$1.36 \cdot 10^{-11}$	$2.19 \cdot 10^{-20}$	$2.04 \cdot 10^{-26}$

Error due to change of transversal field profile

As mentioned in the maintext there is a positional accuracy in placing the near-field probe always at a single position inside a unit cell of the PhC waveguide throughout the measurements. As a consequence, we observe an artificial amplitude modulation in the spectra taken by means of the SNOM. To quantify the possible variation of the signal, we simulate the intensity of the mode inside the PhC waveguide by using MIT Photonics Band Package (MPB).[7] We convolute the calculated intensity profile with a circle of 250 nm to mimic the effect of the aperture size of the near-field probe. The results for the three wavelengths, which are also investigated and modeled in the maintext, are shown in Supporting Figure 2a)-c).

Since we scan the near-field probe transversally over the PhC waveguide to counteract the different extension of the mode profiles visible in the MPB calculations, we integrate the simulated intensity distribution over the x-axis resulting in sinus curves with different modulation depths as shown in Supporting Figure 2d)-f). The error bars, used in Figure 4 in the maintext, are calculated

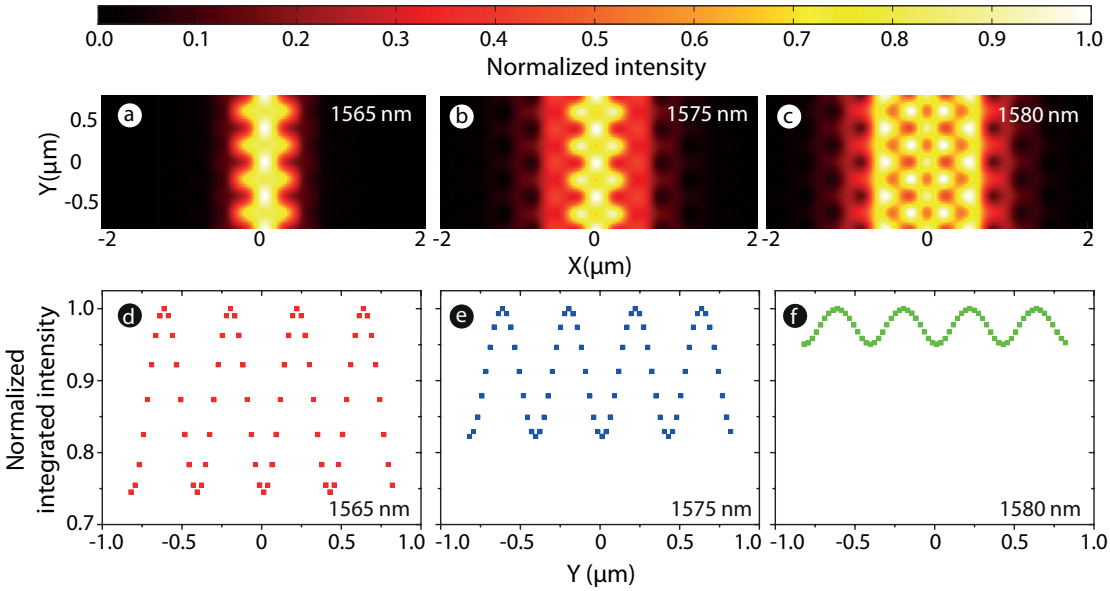

Supporting Figure 2: Calculated intensity distribution convoluted with a 250 nm diameter circle for a wavelength of (a)1565 nm, (b)1575 nm and (c)1580 nm for four unit cells of the PhC waveguide. Corresponding transversally integrated intensity curves.

by determining the ratio of the standard variation to the mean value of these integrated intensity curves, which are listed in Supporting Table 2. It is clear that the intensity profile at the shortest wavelength features the biggest modulation along the propagation direction leading to the largest error bar. For increasing wavelength, the modulation decreases.

Supporting Table 2: Table containing the mean value, standard variation and their ratio for the curves shown in Supporting Figure 2d)-f).

Wavelength	Mean	Standard variation	Ratio
1565 nm	0.87	0.09	10.38 %
1575 nm	0.91	0.063	6.93 %
1580 nm	0.98	0.018	1.8 %

As mentioned in the maintext, the 2 % error bar calculated for the wavelength 1580 nm is too small (cf. Figure 4 in maintext). We attribute this discrepancy to the slow group velocity that the mode inside the PhC waveguide experiences at this wavelength. The slow light enhancement leads to an increased sensitivity of the guided light to possible perturbations. Thus, we estimated an increased background noise level leading to an error bar of 5 %.

References

(1) Reardon, C. P.; Rey, I. H.; Welna, K.; O'Faolain, L.; Krauss, T. F. *J Vis Exp.* **2012**, *69*, E50216.

(2) Li, J.; White, T. P.; O'Faolain, L.; Gomez-Iglesias, A.; Krauss, T. F. *Opt. Express* **2008**, *16*, 6227–6232.

(3) Hugonin, J. P.; Lalanne, P.; White, T. P.; Krauss, T. F. *Opt. Lett.* **2007**, *32*, 2638–2640.

(4) Sinksen, O. V.; Holzlöhner, R.; Zweck, J.; Menyuk, C. R. *J. Lightwave Technol.* **2003**, *21*, 61–68.

(5) LeVeque, R. J. *Finite Difference Methods for Ordinary and Partial Differential Equations*; Society for Industrial and Applied Mathematics, 2007.

(6) O'Faolain, L.; Schulz, S. A.; Beggs, D. M.; White, T. P.; Spasenović, M.; Kuipers, L.; Morichetti, F.; Melloni, A.; Mazoyer, S.; Hugonin, J. P.; Lalanne, P.; Krauss, T. F. *Opt. Express* **2010**, *18*, 27627–27638.

(7) Johnson, S.; Joannopoulos, J. *Opt. Express* **2001**, *8*, 173–190.